Research Paper

Quantitative Image Analysis for Evaluating the Coating Thickness and Pore Distribution in Coated Small Particles

F. L. Laksmana,[1,3,5] L. J. Van Vliet,[2] P. J. A. Hartman Kok,[3] H. Vromans,[3,4] H.W. Frijlink,[1] and K. Van der Voort Maarschalk[1,3]

Purpose. This study aims to develop a characterization method for coating structure based on image analysis, which is particularly promising for the rational design of coated particles in the pharmaceutical industry.

Methods. The method applies the MATLAB image processing toolbox to images of coated particles taken with Confocal Laser Scanning Microscopy (CSLM). The coating thicknesses have been determined along the particle perimeter, from which a statistical analysis could be performed to obtain relevant thickness properties, e.g. the minimum coating thickness and the span of the thickness distribution. The characterization of the pore structure involved a proper segmentation of pores from the coating and a granulometry operation.

Results. The presented method facilitates the quantification of porosity, thickness and pore size distribution of a coating. These parameters are considered the important coating properties, which are critical to coating functionality. Additionally, the effect of the coating process variations on coating quality can straight-forwardly be assessed.

Conclusions. Enabling a good characterization of the coating qualities, the presented method can be used as a fast and effective tool to predict coating functionality. This approach also enables the influence of different process conditions on coating properties to be effectively monitored, which latterly leads to process tailoring.

KEY WORDS: coating; pore size distribution; porosity; quantitative image analysis; thickness distribution.

INTRODUCTION

In the pharmaceutical industry, film coating has been applied for various purposes, such as appearance, taste masking, protection from environmental conditions and sustained or controlled release purposes. Next to the qualitative and quantitative coating formulation, the coating process conditions play an important role in determining the final properties of the coating and its functionality (1). Usually, the appropriate process conditions are difficult to establish after the first development tests. Therefore, in practice, the coating process development involves a lengthy series of experiments characterized by many process adjust-

ments based on the results from the functional tests of the final product.

In the literature, it has often been demonstrated that the coating functionality is correlated with coating properties such as coating thickness and porosity (e.g. (2–5)). For appearance purpose for example, pores in the coating or inhomogeneous coating thickness distributions, both inter-particle and intra-particle may not be a major problem. However, for functionalities that rely on the transport properties through the coating, e.g. extended release or protection, coatings with homogeneous coating thickness distribution and without pores in the coating are needed (4). For this reason, a good characterization of the coating is needed from which the coating functionality can be predicted.

Many coating characterization methods are based on the average values of the total population of particles in a sample, such as the determination of the coating thickness by converting coating mass to thickness (6). However, this approach is not able to give any information on the distribution of the coating and the local coating properties, which are needed for a better prediction of the coating functionality. Functionality tests such as dissolution also do not permit direct correlation with process parameters. Therefore, this work was set out to develop a quantitative image analysis method, which offers an approach to quantify both

[1] Department of Pharmaceutical Technology and Biopharmacy, University of Groningen, A. Deusinglaan 1, 9713 AV, Groningen, The Netherlands.

[2] Department of Imaging Science and Technology, Delft University of Technology, Lorentzweg 1, 2628 CJ, Delft, The Netherlands.

[3] Department of Pharmaceutics, Schering-Plough, PO BOX 20, 5340 BH, Oss, The Netherlands.

[4] Department of Pharmaceutics, Utrecht Institute for Pharmaceutical Sciences (UIPS), Utrecht University, PO BOX 80082, 3508TB, Utrecht, The Netherlands.

[5] To whom correspondence should be addressed. (e-mail: F.L. Laksmana@gmail.com)

overall and local coating properties of a coated particle, i.e. coating thickness distribution and pore size distribution along the particle circumference. These outcomes can be correlated directly to the process conditions used.

The application of quantitative image analysis is common practice in fields like the metal industry to detect mechanical defect of products during processing (7) and in the medical field to evaluate the treatment and drug efficacy (8,9). One of the advantages of image analysis is the possibility to perform visual inspection to validate the analysis results. In spite of its potency, only few papers in literature have described the utilization of quantitative image analysis in a pharmaceutical production environment (10–14). While a terahertz pulsed imaging technique has shown the possibility for measuring the coating thickness distribution on tablets (10–13), our presented method offers the possibility to quantify the complete coating structures, comprising of the thickness and the pore distribution, also on small particles amongst various cores. The quantification method was performed on images acquired using confocal scanning laser microscopy (CSLM), which facilitates the non-invasive visualization of the coating internal structure. This characterization method offers a way to tailor the coating process more effectively.

This paper focuses on the description of the method proposed for the characterization of coating structures, while the correlation between the coating qualities and the process conditions will be the subject of further investigations. We treated the coating, which constitutes polymer and pores, as a film layer formed over a particle. The coating has apparent thicknesses and structures. Pores are defined to be the macroscopic holes within the coating, which are visible with the resolution of the imaging technique used. Further, polymer is defined as the rest of the coating without the visible pores. These terms will be used consistently in this paper.

MATERIALS AND METHODS

Materials

Microcrystalline cellulose/MCC (Avicel PH102, FMC BioPolymer), supplied by Internatio, (Zutphen, the Netherlands) was used as pellet excipient. Hydroxy-propyl methylcellulose/HPMC (Methocel E5 LV USP/ EP premium grade, Dow) supplied by Colorcon (Dartford Kent, UK) was used as coating polymer material. Carmoisine (E122, Pomona BV, Hedel, the Netherlands) was used as pigment in the coating.

Experimental Methods

Pellet Production

The pellets were made in a high shear granulator (Gral 10, Machines Colette, Wommelgem, Belgium), with impeller and chopper rates of 600 and 3,000 rpm, respectively. The pellets were made by mixing 500 g of MCC with 500 g of water, which was poured slowly (in 1 min time) from the top of the Gral. The granulation was performed for 20 min. The wet granules were further dried at 40°C for 8 h in the vacuum drier (Elbanton, Kerkdriel, The Netherlands). Afterwards the pellets were sieved and the fraction 800–1,000 μm was used for further experiments.

Particle Coating

The pellets were coated in the fluidized bed coater (Mycrolab, Oystar Hüttlin, Schopfheim, Germany). 150 g of pellets was used for each batch. The polymer solution can be sprayed either from the bottom or the top of the column. The spray rate in the process using top spray was set at 4.8 g/min while for process using bottom spray, the spray rate was varied at 2.4 g/min and at 4.8 g/min. The rest of the process conditions, i.e. inlet air temperature, inlet air flow rate, atomization pressure, microclimate pressure were kept constant at 70°C, 25 m³/h, 1.5 and 0.6 bar, respectively. The coating process was performed until 20% weight ratio of coating to core was sprayed. The sprayed HPMC solution was HPMC (5% *w/w* in water) and carmoisine (0.1% *w/w* in water) dissolved in cold water and stirring it for about 1 h.

Determination of the Circularity of the Core

The circularity of the MCC pellets was determined using Morphologi G2 from Malvern Instruments (Worcestershire, UK), which was based on the particle image analysis. A LU planar 2.5×/0.075 objective (Nikon, Japan) was used to acquire the particle images. The circularity was calculated using the provided software (Mastersizer ver. 6.0) and was defined as the ratio of the circumference of a circle with the same area as the particle divided by the circumference of the actual particle image.

Image Acquisition

The coating layer was visualized using a Confocal Scanning Laser Microscopy (CSLM). This technique was chosen because of its high spatial resolution and its ability to visualize the internal structure of samples non-invasively by optical sectioning. In this analysis, the carmoisine acts as a fluorescent marker, which permits the visualization of the coating layer and the differentiation of the coating layer from the core. This relies on the good distribution of carmoisine in the HPMC films. This aspect was verified by the absence of hot-spots in the resulted CSLM images, which would have been the signs for inhomogeneous distribution of carmoisine in the HPMC films. Additionally, carmoisine has been used as pigment in diverse HPMC formulations (15–17), where any incompatibility (that leads to separation) between carmoisine and HPMC has not been reported.

The CSLM system used was a Leica inverted microscope DM IRE2 TCS SP2 (Leica microsystems, Germany). A green laser (HeNe 543 nm/1.2 mW) and a red laser (HeNe 633 nm/ 10 mW) were used at 100% and 37.66% intensity settings. A HC Plan Fluotar 10×/0.30 objective was used with a zoom factor of 1 or 10 resulting in scanned areas of 1,500×1,500 μm or 150×150 μm and depth of fields of 50 or 5 μm, respectively. These two optical settings were used to acquire images for the characterization of coating thickness distribution and pore structure, respectively. The emission of the sample was collected at 652–716 nm. The acquired images were 1,024× 1,024 pixels and have a gray resolution of 8 bit. Immersion oil

type B (Cargille Lab, USA) was added to the coated particles prior to scanning. No interaction between the HPMC polymer and the immersion oil used is expected as HPMC is known as a barrier material against oils (18). For every sample from different process conditions, the images for the thickness determination were taken from three different particles. From each particle two images were taken from two random sides of the coating for the characterization of the pore structure.

Quantitative Image Analysis

The quantitative image analysis was performed using the image processing toolbox provided in MATLAB R2007a. The quantification comprised the determination of the coating thickness distribution, the porosity and the pore size distribution.

Coating Thickness Distributions

A typical CSLM image acquired for the coating thickness analysis is shown in Fig. 1A. Before the images were ready to be used for the thickness analysis, several steps had to be performed, comprising the image contrast enhancement and the image binarization. The contrast enhancement was performed using Contrast-Limited Adaptive Histogram Equalization (ADAPHISTEQ) command in the MATLAB image processing toolbox. In this work, a tile size of 15× 15 pixels was used, and the corresponding result of the contrast enhancement on the given image example is shown in Fig. 1B. The results and discussion section gives a justification for the choice of these settings.

The image binarization was performed by using the Isodata threshold algorithm (19). In the resulted binary images, the pore and the polymer pixels have the intensity of '0' (black) and '1' (white), respectively, such as shown in Fig. 1C. Afterwards, the pores within the coating were closed, i.e. the pixel of the pores were set to '1' (Fig. 1D). This means that the coating thickness was defined as the total (apparent) thickness including the pores inside the coating.

There are three algorithms that were used to determine the coating thickness distribution, the "Radius" method and two variations of the "Euclidean distance" method. In the "radius" method, the thickness analysis started by determining the centre of the particle (called centroid), and the inside boundary (facing the core) and the outside boundary (facing the background) of the coating layer, such as shown in Fig. 1E, F, respectively. The centroid was determined using the REGIONPROPS command, while the coating boundaries were determined using the BWBOUNDARIES command provided in the MATLAB image processing toolbox. The number of the inside and outside boundary pixels is typically above 1,500, which varies slightly depending on the particle and coating roughness. The centroid and each of the inside boundary points were then connected with straight lines. This was repeated for all outside boundary pixels, as illustrated in Fig. 2 (left). The length of the line segments connecting the centroid-outside boundary and the centroid-inside boundary that run in the same direction are subtracted from each other. The results were taken as the coating thickness. In this way, the variation of the coating thickness along the particle circumference was measured, as depicted in Fig. 2 (right).

From the thickness measurements, we built a coating thickness distribution and a cumulative thickness distribution per particle, which form the basis for a statistical analysis. We obtained the estimation for the minimum coating thickness and the span (width) of the coating thickness distribution were also derived. The relative span of the coating thickness is defined as

$$\text{Span} = \frac{\Delta X_{n,90\%} - \Delta X_{n,10\%}}{\Delta X_{n,50\%}} \quad (1)$$
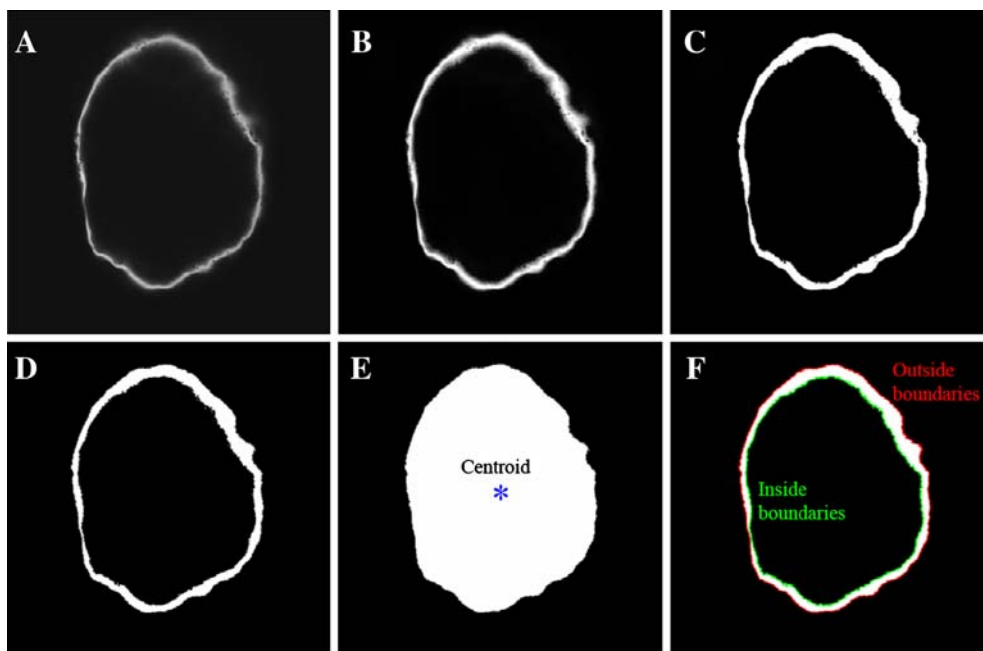

Fig. 1. Image processing steps for the coating thickness characterization. **A** Raw image. **B** After contrast enhancement. **C** After binarization. **D** After filling the pores within the coating. **E** Determining the centroid. **F** Determining the outside and inside boundaries.
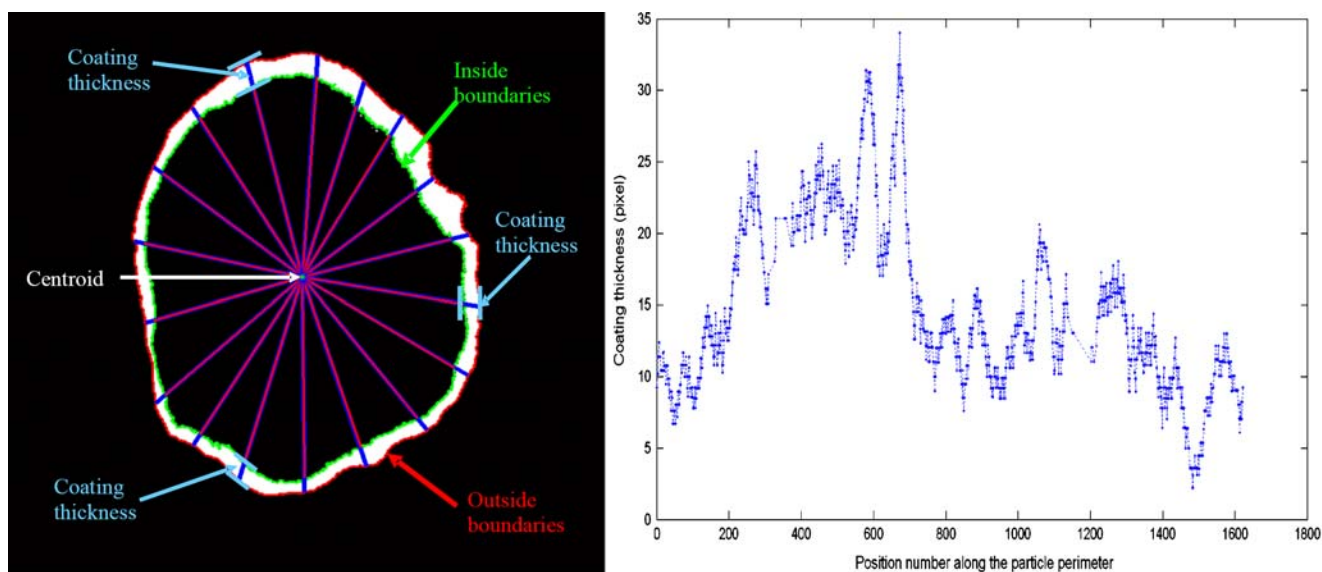
Fig. 2. Schematic figure on how the coating thickness was determined using the present image analysis.

where , $\Delta X_{n,10\%}$, $\Delta X_{n,50\%}$, $\Delta X_{n,90\%}$ are the percentiles of the (number) thickness distribution at respectively 10%, 50% (median) and 90%.

The two "Euclidean distance" methods measure the minimum coating thickness from each pixel on the inner to the outer boundary of the coating or vice versa. In this paper, the coating thickness was mainly measured using the "radius" method. The "Euclidean distance" methods have been used as an alternative for the "radius" method. The results from these methods are compared and presented in the results and discussion section.

Quantification of the Porous Structure

Before pore characterization, the contrast of the CSLM images was enhanced and the images were transformed from gray-scale to binary images in a way similar to the procedure for the coating thickness analysis. Fig. 3A–I show the typical transformation results after the subsequent image processing steps for the pore characterization. Due to the complexity of the porous structure, a different method (i.e. based on Fuzzy c-means cluster) was used during the image binarization. In this algorithm, the pixel intensities were classified into n ($n \geq 3$) clusters using the Fuzzy Clustering method (20,21). These clusters have mean intensities that increase from the lowest (cluster 1) to the highest (cluster n). This paper used two thresholds during the image binarization: the threshold between cluster 1 and 2 (called the lower threshold) and the threshold between cluster 2 and 3 (called the higher threshold). The typical binarization results of using lower and higher thresholds are presented in Fig. 3C,D. The colors red and blue were added to these images (also to Fig. 3G) to aid the illustration of the coating and pore boundaries, respectively. Using the lower threshold value, only pixels that are very dark (low intensity) are segmented as pores or otherwise they would be segmented as polymer. This thresholding results in a more accurate determination of the coating boundaries (see Fig. 3C). In contrast, using the higher threshold value, more pores are visible, while some portion of the polymer disappears, as only

the very bright pixels (having high intensity) are segmented as polymer (see Fig. 3D).

Therefore, the next step was taken to combine the binarization results using lower and higher thresholds in order to obtain a binary image, which closely resembles the raw image. As the coating segmented using lower threshold (Fig. 3C) is bigger than the coating segmented using higher threshold (Fig. 3D), the algorithm started by defining the difference between these two binarized images, resulting in Fig. 3E. Afterwards, the intersection between the images obtained using the two thresholds was determined, resulting in Fig. 3F. This implies that only the polymer pixels that exist in both images (Fig. 3D,E) are taken, which otherwise are taken as black pixels in the new figure (Fig. 3F). As a result, all pores present in both images within the coating boundaries (i.e. segmented using the higher threshold) are shown in the new image (Fig. 3F). The last step was to add the images obtained from these two steps (Fig. 3E,F), which result is shown in Fig. 3G. Mathematically, the algorithm that combines the images can be written as:

$$Fig3G = Fig.3E + Fig.3F \qquad (2)$$
$$= (Fig3C - Fig3D') \cup (Fig3C \cap Fig3D)$$

where the first and the second terms in the equation are equal to Fig. 3E,F, respectively. Fig. 3D′ is an image obtained after filling the pores (removing the pores) in Fig. 3D with white pixels.

In some images, some white pixels can be found disconnected from the rest of the coating, either outside the main coating or inside the pores, as shown in Fig. 3G. These disconnected pixels, further called "loose pixels" were considered differently, dependent on their spatial distance to the main coating. If they are very close, they were considered to be a part of the coating, which was disconnected during image binarization due to the presence of surrounding polymer pixels with a low intensity as a result of the so called "partial volume effect" between them. However, if they are quite far from the main coating or inside the pores (so called
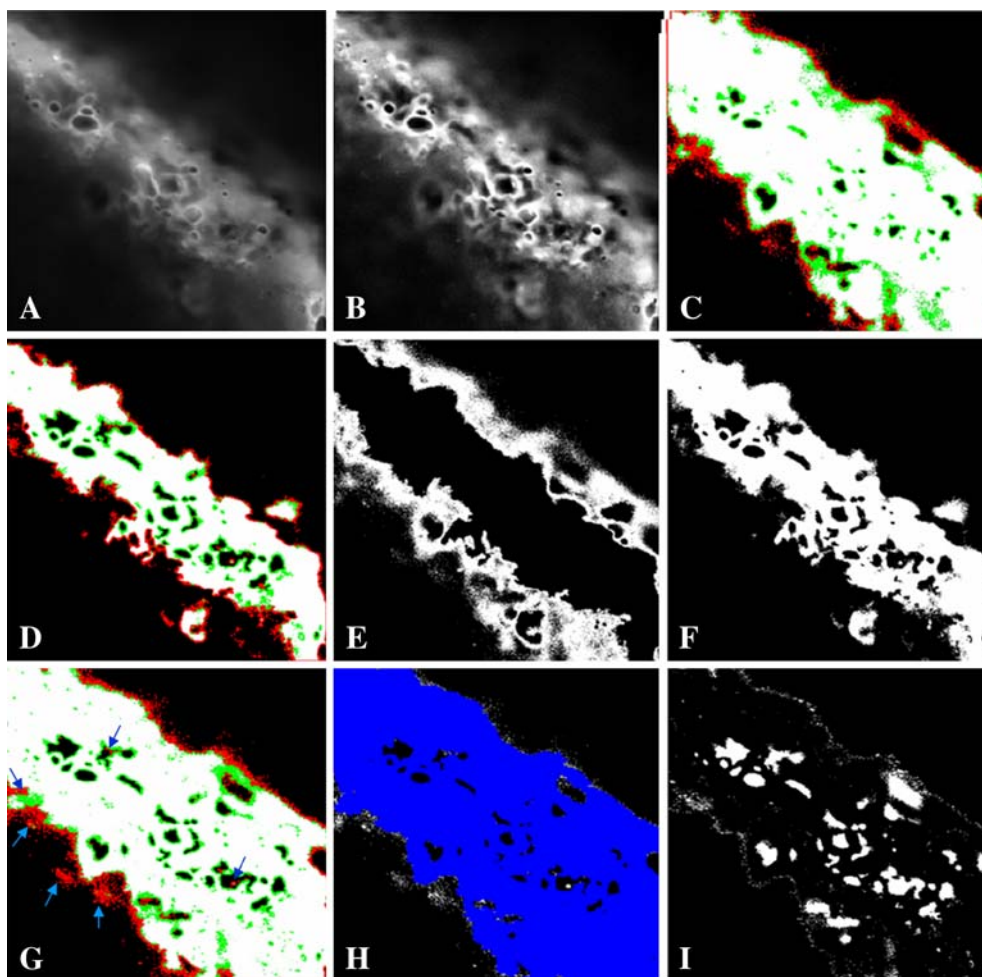
Fig. 3. Image processing steps for the pore characterization: **A** Raw image. **B** After contrast enhancement. **C** Binarization result using a threshold between low and medium intensity clusters. **D** Binarization result using a threshold between medium and high intensity clusters. **E** Image resulted after filling the pores in image **D** and subtracting the obtained image from image **C**. **F** Image resulted after intersecting image **C** and **D**. **G** Image resulted after adding image **E** and **F**. *Red and green colors* indicate the coating and the pore boundaries, respectively. **H** After selecting only the connecting pixels. *Blue color* indicates the analyzed coating region. **I** After removing the floating pixels inside the pores and taking the pores out of the coating.

"floating pixels"), they can not physically be a part of the coating and hence were considered as image noise. Therefore, an extra operation was performed to connect only the nearby loose pixels to the main coating and to exclude the distant loose pixels and the loose pixels in the pores from the analysis. To connect the nearby loose pixels to the main coating, a closing (a dilation followed by erosion) operation was performed (22). By selecting only the pixels between the connecting coating and pore boundaries, the rest of the loose pixels were automatically removed. The result example of this operation is shown in Fig. 3H. The blue shade reflects the area of the polymer, which was used for the analysis. The quantification of the porosity was then performed on this image.

Porosity. The coating does not cover the whole area of the image, of which a large proportion is constituted by the background and the particle core (here the particle core was also considered as background). This background is indistinguishable from the pores based on the pixel intensity. Therefore extra procedure was performed to separate the pores from the

coating. This was performed by inversing the image thereby the pores become the true elements of the image and followed by inversing only the background back from white to black pixels. The result of this step is shown in Fig. 3I, where pores are shown as white pixels and the rest of the coating and the background shown as black pixels. Using this image, the porosity was quantified. The area of the pores was determined by calculating the area of the pores, which have been segmented from the coating (Fig. 3I). The porosity was then calculated by dividing the area of pores by the area of the coating, which was the total area of the polymer and the pores.

$$\text{Porosity} = \frac{\text{Area of pores}}{\text{Area of coating}}$$
$$= \frac{\text{Area of pores}}{\text{Area of polymer} + \text{Area of pores}} \quad (3)$$

Pore Size Distribution. The pore size distribution was measured by using a method from image processing called "a
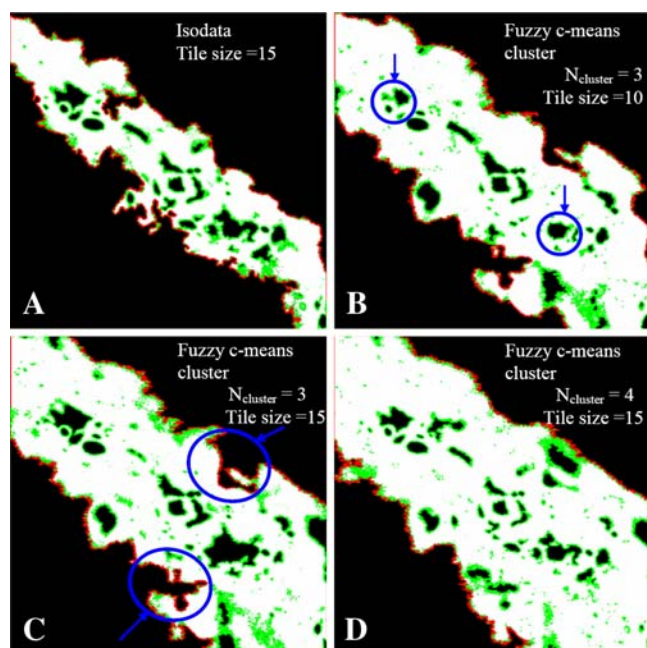
Fig. 4. Comparison in the binarization results by using different thresholding and image preparation settings. **A** Using Isodata thresholding. **B** Using tile size = 10 during image contrast enhancement **C** and **D** Using three and four clusters during fuzzy c-means cluster thresholding, respectively. *Red and green colors* indicate the coating and the pore boundaries, respectively.

morphological sieve" as used by Wu *et al.* (14). The principle of the approach has been comprehensively described and can be found in the original paper. The granulometry was performed on the images obtained after pore separation procedure (Fig. 3I). By applying closings with structuring element with increasing size, the pores progressively disappear and the remaining area of the white pixels at each size step was computed. As the result, a curve between the area of the white pixels (the area of pores) and its corresponding structuring element size (pore size) was derived. The difference between the area of the white pixels at certain pore size and the area of the white pixels at one step pore size behind is the area of the pore at its corresponding size. The results were normalized with the total area of pores and presented as the cumulative relative area distribution of the pore size.

RESULTS AND DISCUSSION

Image Preparation: Image Binarization

After the phases in the image, i.e. pores, polymer and background are well segmented, the quantification can readily be performed. Therefore, the binarization step is very critical as the quantification results are dependent on the segmentation results. One of the advantages of using image analysis is the possibility to perform the evaluation of the method visually.

Fig. 4A,D show the differences in the binarization results using two different threshold selection methods: Isodata *versus* Fuzzy c-means cluster, respectively. It can be seen that the binary image obtained using fuzzy c-means cluster thresholding, resembles the original image better than the Isodata method.

Additionally, the tile size used during the image contrast enhancement and the number of clusters used during thresholding were found to be important, as illustrated in Fig. 4B–D. Here, it can be seen using tile size 10×10 pixels (Fig. 4B), less pores are segmented than using the thresholding conditions used in Fig. 4(D). Using three clusters in the fuzzy c-means cluster thresholding (Fig. 4C), a small portion of coating is not visible in the resulting binary image. At different combination of thresholding conditions, the resulted binary images were visually compared. In this way, the tile size and the number of clusters used were optimized. The chosen settings for the tile size and the number of clusters are 15×15 pixels and 4, respectively. Considering their significant
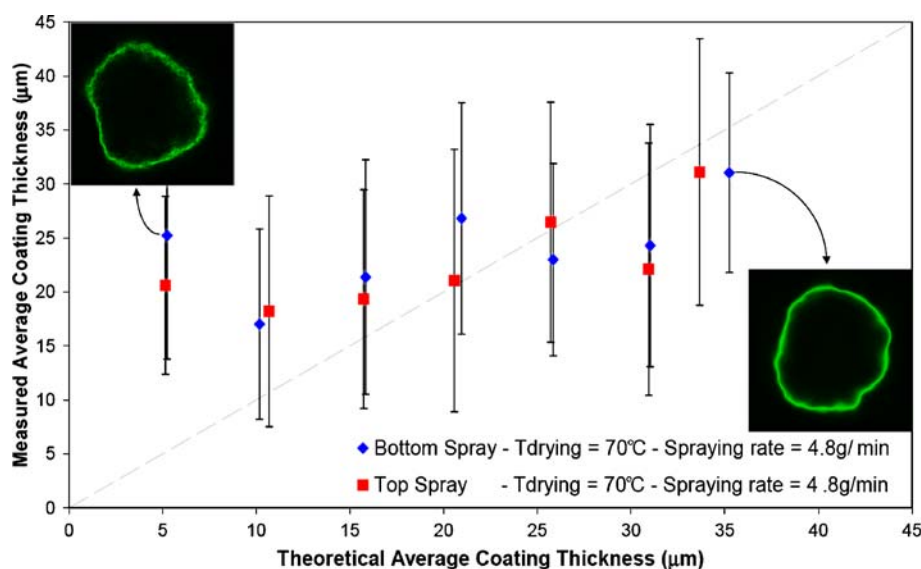

Fig. 5. Comparison between the theoretical average coating thickness with the average coating thickness measured using the present method. The theoretical average of coating thickness was calculated from the amount of coating solution sprayed to the particles, according to Eq. 4.
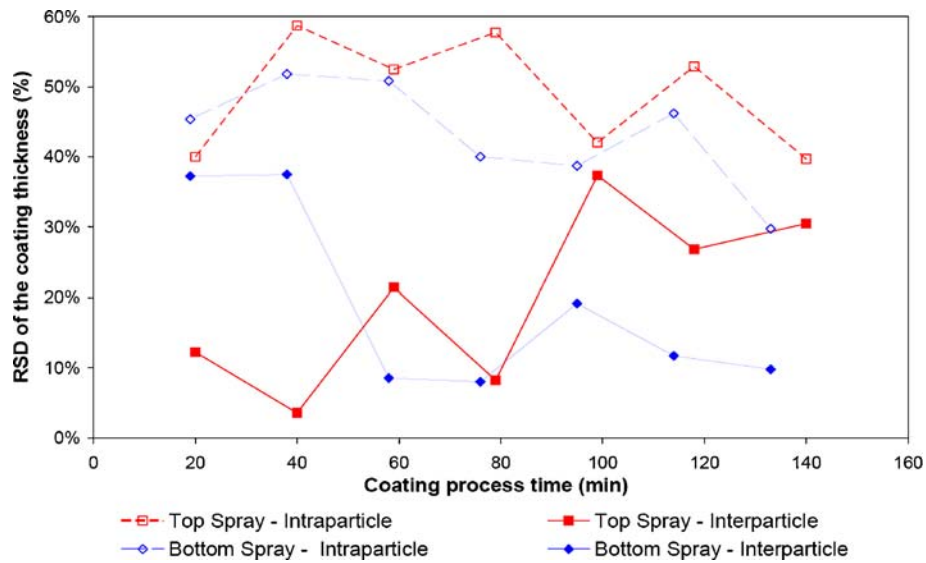
Fig. 6. Comparison between the relative standard deviation of coating thicknesses within one particle (intraparticle) and between particles (interparticle).

influence on the quantification results, values were kept constant in this study.

Evaluation of the Characterization of the Coating Thickness Distribution

The average coating thickness measured using the present method and the theoretical average coating thickness were compared, the results are shown in Fig. 5. Here,

examples are taken from the coating made in the fluidized bed using bottom and top spray systems. In this paper, the theoretical coating thickness was calculated from the amount of coating polymer sprayed in a certain time, following Eq. 4. In this equation, $\Delta x_{\text{theoretical}}$, F_{spray}, t, C_{pol}, m_{bed}, d_{core}, ρ_{core} and ρ_{pol} are the coating thickness, the mass spraying rate of the coating solution, the process time, the polymer concentration in the coating solution, the total mass of the core particles to be coated, the average diameter of the core

Table I. Comparison Between the Radius Method (Taking Coating Thickness as the Radius from Inside to Outside Boundaries) and Euclidean Distance Methods (Taking the Coating Thickness as the Euclidean Distance from Inside to Outside Boundaries and Vice Versa)

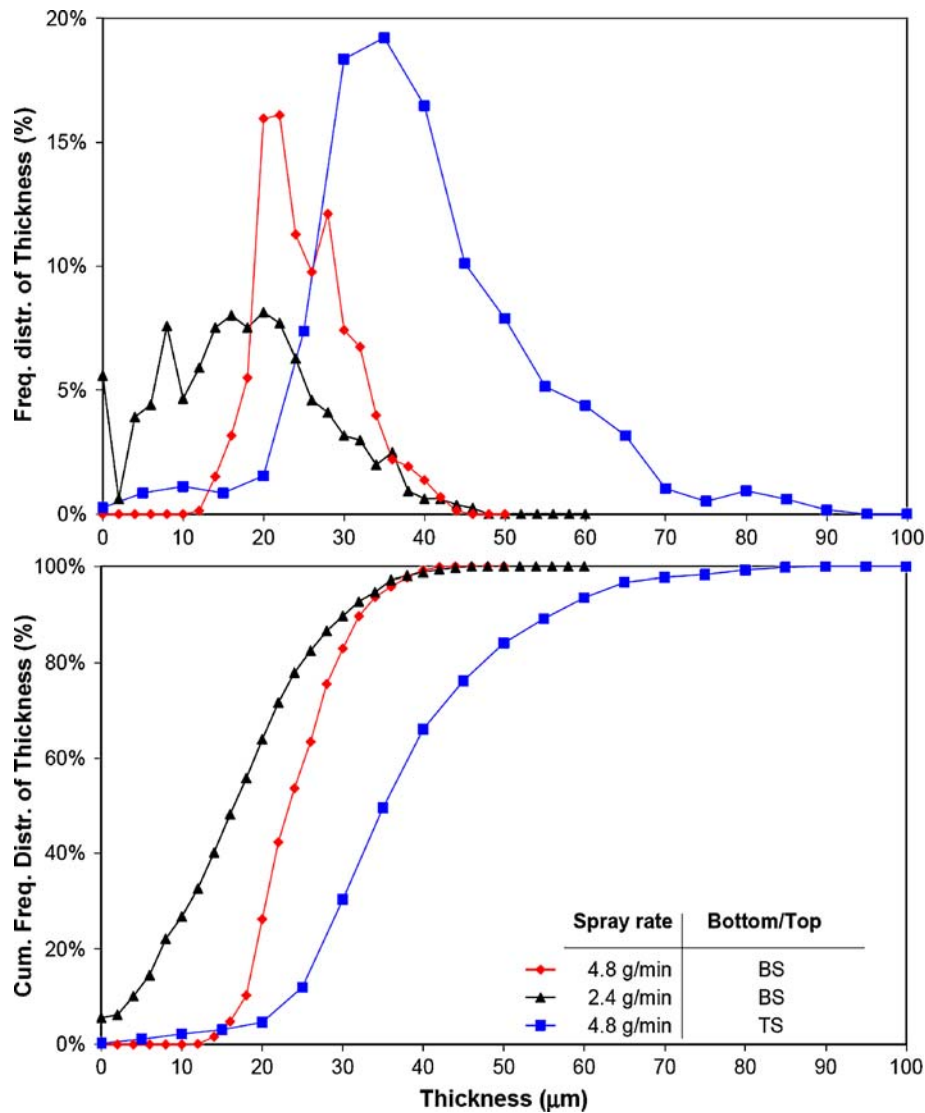|		Radius from inside to outside boundaries	Euclidean distance from inside to outside boundaries	Euclidean distance from outside to inside boundaries
Non-porous coating				
	Δx_{min} (μm)	8.1576	7.1821	7.2599
	Δx_{avg} (μm)	28.5833	27.0241	25.9347
	Δx_{max} (μm)	53.2246	44.4882	45.3939
	Span (-)	0.8611	0.8115	0.8772
Porous coating				
	Δx_{min} (μm)	13.3263	9.5596	10.9288
	Δx_{avg} (μm)	33.7355	28.5607	27.4527
	Δx_{max} (μm)	78.9115	58.69	64.157
	Span (-)	1.2478	0.9892	1.2187

Fig. 7. Examples of the obtained coating thickness (frequency) distribution.

particles and the true density of the core and coating polymer, respectively.

$$\Delta x_{theoretical} = \frac{F_{spray} \times t \times C_{pol} \times \rho_{core} \times d_{core}}{6 \times m_{bed} \times \rho_{pol}} \qquad (4)$$

It can be seen in Fig. 5, that the measured thicknesses do not always correspond well with the theoretical thicknesses,

especially at low theoretical thicknesses (coating thicknesses after a short spraying time). In the present approach, the porosity was also included into the determination of the coating thickness (see Section Coating Thickness Distributions). In the beginning of the coating process, the coating film is very porous (see the CSLM image inserted in Fig. 5 top-left corner). Furthermore, it can be noticed in this figure that the coating thickness does not increase significantly with the spraying time. This effect is actually due to the reduction of the porosity in time, which is

Table II. The Effects of Varying the Nozzle Position and Spraying Rate on the Coating Qualities

Nozzle position	Bottom	Bottom	Top
Spraying rate (g/min)	2.4	4.8	4.8
Minimum coating thickness (μm)	0±6.87	18.68±5.65	3.82±2.82
Average coating thickness (μm)	28.08±10.36	31.04±3.04	31.10±9.48
Maximum coating thickness (μm)	56.74±9.27	64.62±4.75	72.59±15.35
Relative span of coating thickness distribution (−)	1.48±0.81	0.80±0.17	1.26±0.15
Total porosity (%)	3.38±0.60	3.03±0.37	6.77±0.43
Average pore size (μm)	0.50	0.51	2.28
Pore size at which 90% (number based) of the pores are undersized, $d_{pore,90}$ (μm)	0.91	1.12	6.01

indicated in the CSLM image of the coating sample taken from the end of coating process (see Fig. 5 top-right corner). This particular subject will be discussed further in a separate paper.

Measuring the thickness along the particle circumference shows the inhomogeneity of the coating thickness on each particle, i.e. intra-particle standard deviation of the coating thickness. Additionally, among different particles, the average thickness and the span of the distribution may also differ, resulting in a degree of inter-particle standard deviation of the coating thickness.

Fig. 6 shows the difference in the intra-particle and inter-particle variations of the coating thickness, which belong to the coatings made with bottom and top spray given as examples. A batch with small variation in the average coating thickness between particles does not assure a narrow coating thickness distribution of each particle. When it happens that the intra-particle variation of the coating thickness is high, the characterization of the intra-particle distribution becomes more critical, as it is the one that is responsible for determining the coating functionality. It is shown in Fig. 6 that in general the variations in the coating thickness on each particle are higher than the variations of the coating thickness between the particles. This is valid even for coating film made using top-spray system, which has high inter-particle variation in the thickness. Therefore, in the present situation, the focus will be on the intra-particle variation of the coating thickness.

Table I shows the results of using the "radius" method for determining the coating thickness distribution, which is compared to other possible methods: taking the coating thickness as the "Euclidean distance" from the inside to the outside boundaries and vice versa. Here, examples are taken from coatings made from processes using spraying rate of 4.8 g/min where the nozzle was positioned either at the bottom or the top of the fluidized bed column. These coating conditions lead to two different coating morphologies: a non-porous and a porous coating.

It can be seen in Table I that the coating thicknesses determined using the "radius" method are higher than the ones determined using the "Euclidean distance" methods. For porous coating, the span of the coating thickness distribution determined using the "radius" method is higher than the one determined using the "Euclidean distance" methods. The "Euclidean distance" methods always look for the shortest distances from inside to outside boundaries or vice versa. In this way, the complete curvature of the coating layer can not be identified as some points at the coating boundaries are skipped (as pointed by the arrows). Therefore, particularly for a coating with large thickness variation, the "Euclidean distance" method is not able to give the true thickness distribution. In contrast, the "radius" method covers all boundary points of the coating (including along protrusions of the coating), therefore giving a better estimation of the
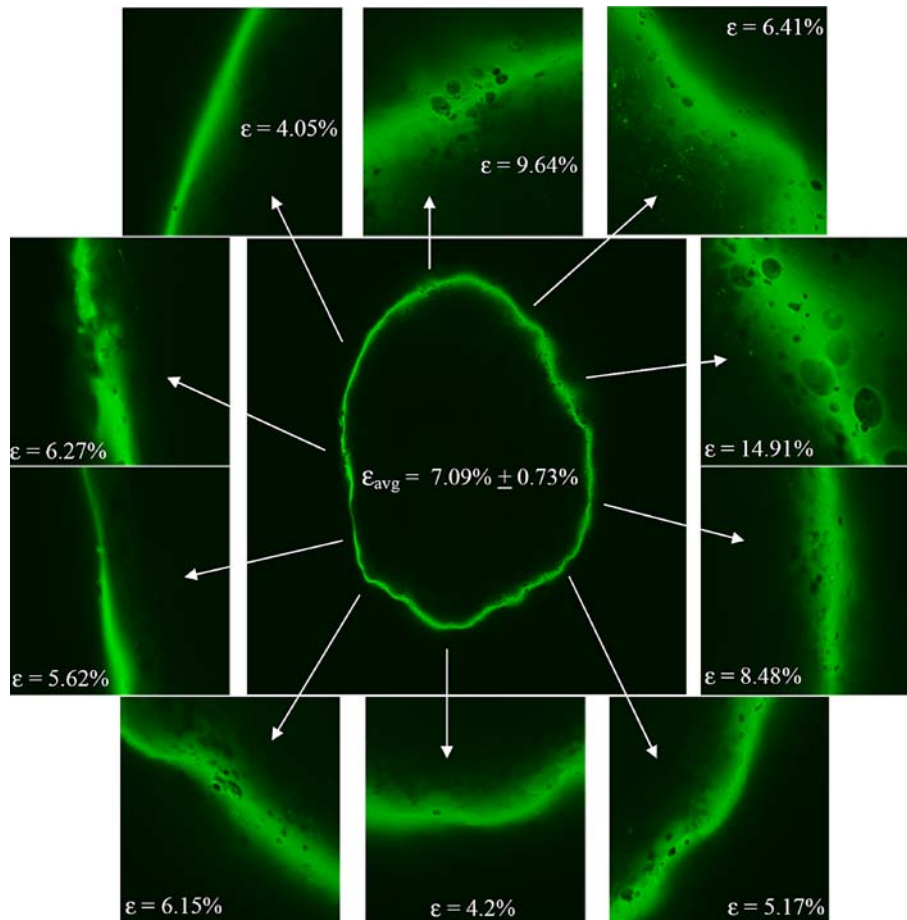

Fig. 8. Inhomogeneity of the coating structures.

variation in the coating thickness. A disadvantage of the "radius" method is that the boundary thickness is measured along a path through the object's centroid. This does not guarantee that the measurement is performed perpendicular to the local contour especially for roughly shaped particles.

Nevertheless, the Euclidean distance method has a particular advantage. The way that the Euclidean distance method always seeks for the minimum distance from one boundary point to another is analogous to the phenomena occurring during the functioning of the coating, e.g. the diffusion of active substance from the core to the environment through the coating membrane or the diffusion of moisture and oxygen from the environment to the core.

Being aware of both the advantages and the disadvantages of the possible methods used to determine the coating thickness, it was decided to use the "radius" method in this paper. The reason was because this method is more sensitive in revealing the variation in the coating thickness distribution, which is our current interest. This information can then be used to investigate the effect of different process conditions. Moreover, the values of the

minimum coating thicknesses obtained using the different methods appeared to be in the same order of magnitude (Table I).

Examples of the characterized coating thickness distributions are shown in Fig. 7, taken from particles coated at low (2.4 g/min) and high (4.8 g/min) spraying rates using bottom spray and high spraying rate using top spray. The samples were taken after similar amount of coating solution were sprayed. It is shown that the thickness distributions of the coating made at these three different conditions are clearly distinguished. The minimum, average and maximum coating thickness and the span of the coating thickness distribution were also derived and are depicted in Table II. Coatings with the same average thickness can appear to have significantly different minimum thickness, as found in the thickness properties of these three different coatings (see Table II). The imperfect coverage of the particles coated at low spraying rate was clearly visible, i.e. the minimum thickness is zero. Furthermore, it is possible to calculate the fraction of the total surface of the particle which is not covered by the coating from the frequency distribution of the coating
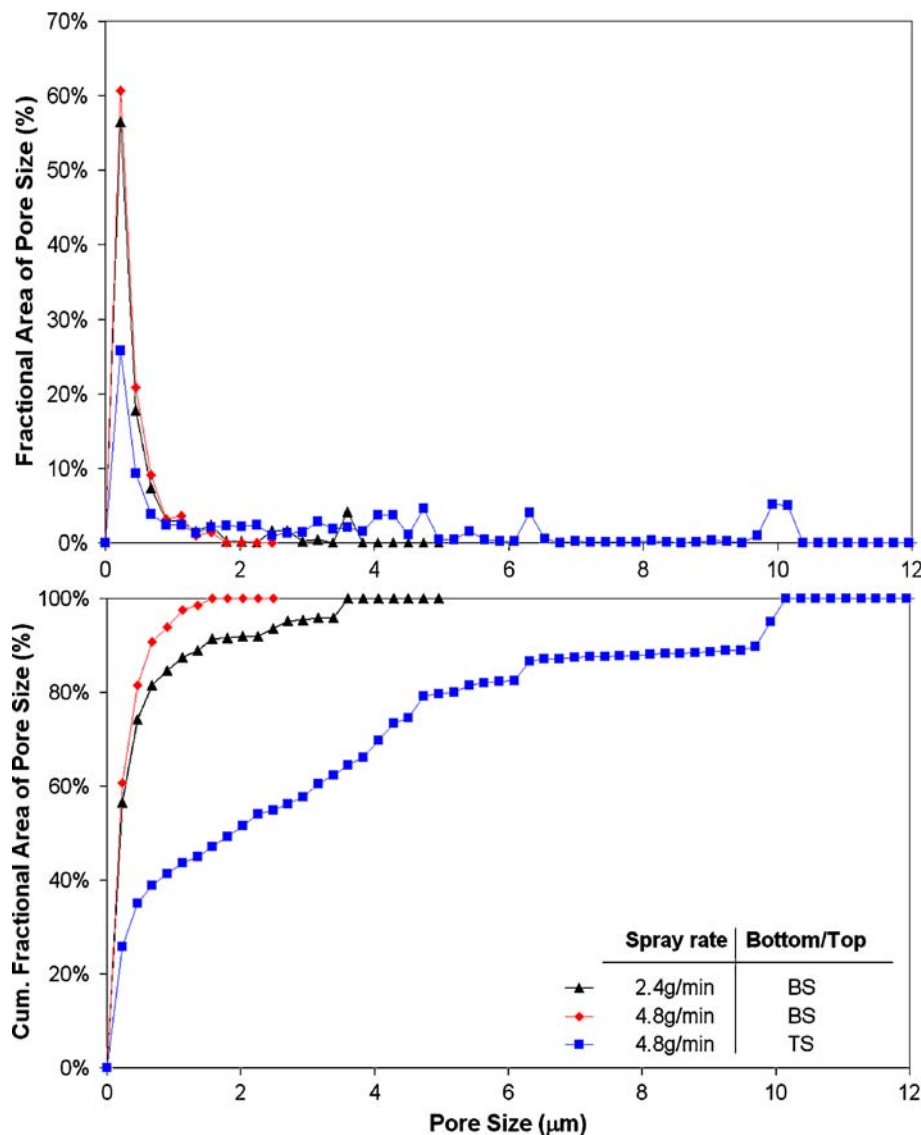

Fig. 9. Examples of the obtained pore size (area) distribution.

thicknesses. In the case of sample coated at low spraying rate, this fraction is around 6% (Fig. 7). This ability to quantify the difference in the minimum coating thickness enable the anticipation of coating functionality failure due to the presence of a very thin local thickness.

The large variation between the minimum and the maximum thickness of the coating made at a low spraying rate is also shown in the higher span of the thickness distribution. This parameter shows the variation of the coating thickness along the particle perimeter. Additionally, the inter-particle variation (shown as the error range of the thickness properties) of the coating film made at a low spraying rate is also the largest. On the other hand, the variations are lower in coating made using a higher spraying rate. By using these characterization results, the appropriate adjustments can be made with regards to the process coating conditions.

Evaluation of the Characterization of the Coating Porosity

The reliability of the current analysis method for the characterization of the pore structure was also evaluated. For this reason, extra samples were taken from particles coated using the top spray method, from which 10 images at random positions along the particles perimeter were taken and quantified, as shown in Fig. 8. This coated particle was chosen as it represents the most inhomogeneous pore structure found in the coating. The average porosity determined from 10 images is 7.1% and the porosity values from each image can deviate to about 10% relative to the average value. Using the current sampling method, where 6 images were used comprising two images from three different particles, the average porosity for this coated particle was found to be 6.3%, with relative deviation to about 14% of the average value. This difference due to the sampling limitation is systematically present in every compared batch, which therefore will not alter the interpretation of the data.

Evaluation of the Characterization of the Pore Size Distribution

In order to make a more detailed study of the porous structure the pore size distribution of the coating has been determined. The advantage of the present image analysis is that not only the porosity but also the pore size distribution can be quantified. Examples of the characterization results are depicted in Fig. 9, showing the derived fractional area and cumulative distributions of the pore size. It can be seen that coating sprayed using the top spray has a wide variation in pore size. This data should be used together with the porosity data to fully evaluate the pore structure of the coating, such as depicted in Table II. From this result, it can be verified that the coating made using top spray not only has a higher porosity but also possesses a bigger pore size, compared to the coating made using bottom spray.

Furthermore, the characterization of coating structure presented in this paper is non-invasive. This is of course preferable as many other methods require some preparation steps e.g. cutting or embedding of the coating layer, which may alter the coating structure.

CONCLUSIONS

It has been demonstrated, that using the presented image analysis methods, the coating thickness distribution along the particle perimeter, the porosity and also the pore size distribution can be adequately quantified. These parameters are the determining factors for the coating properties and functionality. From the examples given, it has also been illustrated how the influence of different process conditions on the coating properties can be monitored using the presented approach. Further work is ongoing to develop a correlation between the process settings and the coating qualities, from which the coating characterization results can be proposed to be used as a feedback to control the coating process to assure a coating product with the desired quality.

REFERENCES

1. S. Missaghi, and R. Fassihi. A novel approach in the assessment of polymeric film formation and film adhesion on different pharmaceutical solid substrates. *AAPS PharmSciTech.* **5**:32–39 (2004). doi:10.1208/pt050229.
2. F. Debeaufort, M. Martin-Polo, and A. Voilley. Polarity homogeneity and structure affect water vapor permeability of model edible films. *J Food Sci.* **58**:426–434 (1993). doi:10.1111/j.1365-2621.1993.tb04290.x.
3. J. M. Lagaron, R. Catala, and R. Gavara. Overview: structural characteristics defining high barrier properties in polymeric materials. *Mater Sci Technol.* **20**:1–7 (2004). doi:10.1179/026708304225010442.
4. E. Kleinbach, and Th. Riede. Coating of Solids. *Chem Eng Process.* **34**:329–337 (1995). doi:10.1016/0255-2701(94)04021-4.
5. A. Jarosiewicz, and M. Tomaszewska. Controlled-release NPK fertilizer encapsulated by polymeric membranes. *J Agric Food Chem.* **51**:413–417 (2003). doi:10.1021/jf020800o.
6. B. Guignon, E. Regalado, A. Duquenoy, and E. Dumoulin. Helping to choose operating parameters for a coating fluid bed process. *Powder Technol.* **130**:193–198 (2003). doi:10.1016/S0032-5910(02)00265-6.
7. S. N. Eremin. Image processing technology in the systems for quality control of sheet metal roll. *Pattern Recognit Image Anal.* **16**:127–130 (2006). doi:10.1134/S1054661806010408.
8. D. Sahani, S. Saini, G. A. Fatuga, E. F. Halpern, M. E. Lanser, J. B. Zimmerman, and A. J. Fischman. Quantitative measurements of medical images for pharmaceutical clinical trials: comparison between on-site and off-site assessments. *AJR Am J Roentgenol.* **174**:1159–1162 (2000).
9. S. D. Pathak, L. Ng, B. Wyman, S. Fogarasi, S. Racki, J. C. Oelund, B. Sparks, and V. Chalana. Quantitative image analysis:

software systems in drug development trials. *Drug Discov Today.* **8**:451–458 (2003). doi:10.1016/S1359-6446(03)02698-9.

10. L. Ho, R. Müller, M. Römer, K. C. Gordon, J. Heinämäki, P. Kleinebudde, M. Pepper, T. Rades, Y. C. Shen, C. J. Strachan, P. F. Taday, and J. A. Zeitler. Analysis of sustained-release tablet film coats using terahertz pulsed imaging. *J Control Release.* **119**:253–261 (2007). doi:10.1016/j.jconrel.2007.03.011.

11. L. Ho, R. Müller, K. C. Gordon, P. Kleinebudde, M. Pepper, T. Rades, Y. C. Shen, P. F. Taday, and J. A. Zeitler. Applications of terahertz pulsed imaging to sustained-release tablet film coating quality assessment and dissolution performance. *J Control Release.* **127**:79–87 (2008).

12. J. A. Spencer, Z. M. Gao, T. Moore, L. F. Buhse, P. F. Taday, D. A. Newham, Y. C. Shen, A. Portieri, and A. Hussain. Delayed release tablet dissolution related to coating thickness by terahertz pulsed image mapping. *J Pharm Sci.* **97**:1543–1550 (2008). doi:10.1002/jps.21051.

13. J. A. Zeitler, Y. C. Shen, C. Baker, P. F. Taday, M. Pepper, and T. Rades. Analysis of coating structures and interfaces in solid oral dosage forms by three dimensional terahertz pulsed imaging. *J Pharm Sci.* **96**:330–340 (2007). doi:10.1002/jps.20789.

14. Y.-S. Wu, L. J. Van Vliet, H. W. Frijlink, and K. Voort Maarschalk. Pore size distribution in tablets measured with a morphological sieve. *Int J Pharm.* **342**:176–183 (2007). doi:10.1016/j.ijpharm.2007.05.011.

15. T. A. Hollowood, R. S. T. Linforth, and A. J. Taylor. The effect of viscosity on the perception of flavour. *Chem Senses.* **27**:583–591 (2002). doi:10.1093/chemse/27.7.583.

16. G. S. Bajwa, K. Hoebler, C. Sammon, P. Timmins, and C. D. Melia. Microstructural imaging of early gel layer formation in HPMC matrices. *J Pharm Sci.* **95**:2145–2157 (2006). doi:10.1002/jps.20656.

17. A. Reitnauer. A method of forming a mark on a product. 07024129.4[EP1 914 280 A1]. 2007.

18. H. L. Huse, P. Mallikarjunan, M. S. Chinnan, Y.-C. Hung, and R. D. Phillips. Edible coatings for reducing oil uptake in production of akara (deep-fat frying of cowpea paste). *J Food Process Preserv.* **22**:155–165 (2007). doi:10.1111/j.1745-4549.1998.tb00811.x.

19. T. W. Ridler, and S. Calvard. Picture thresholding using an iterative selection method. *IEEE Trans Syst Man Cybern.* **8**:630–632 (1978). doi:10.1109/TSMC.1978.4310039.

20. W. E. Phillips II, R. P. Velthuizen, S. Phuphanich, L. O. Hall, L. P. Clarke, and M. L. Silbiger. Application of fuzzy c-means segmentation technique for tissue differentiation in MR images of a hemorrhagic glioblastoma multiforme. *Magn Reson Imaging.* **13**:277–290 (1994). doi:10.1016/0730-725X(94)00093-I.

21. Y. Yong, Z. Chongxun, and L. Pan. A novel fuzzy c-means clustering algorith for image thresholding. *Meas Sci Rev.* **4**:11–19 (2004).

22. I. T. Young, J. J. Gerbrands, and L. J. Vliet. *Fundamental of Image Processing*. Delft University of Technology, Delft, 1998.